

# Investigating Multivariate, Vector, and Topological Data Analysis Techniques for Mantle Flow Pattern Visualization

Sudhanshu Sane\*

Tushar M. Athawale†

Chris R. Johnson‡

SCI Institute at University of Utah

## 1 INTRODUCTION

The Earth’s mantle convection data is discretized on a curvilinear grid with multivariate data consisting of scalar as well as vector field data and consists of 250 time slices 2 Myr apart. Prior studies of mantle flow patterns [9–11], as well as works prioritizing mantle convection visualization [1, 3, 6–8, 13], have employed time-varying 2D slices, 3D isosurfaces, or volume rendering for the visualization of univariate scalar fields and glyph-based techniques for flow visualization. We demonstrate the use of feature level-sets (isosurface-based multivariate data visualization technique), attribute-filtered integral curves (streamlines and pathlines), and topological analysis to study mantle flow patterns. We briefly describe each of these approaches in Section 2, and present our finding using these methods in Section 3.

## 2 VISUALIZATION AND ANALYSIS TECHNIQUES

We consider three categories of techniques to study the data set: isosurface-based techniques, flow visualization techniques, and topological data analysis techniques. We use the *temperature anomaly*, spin transition-induced *density anomaly*, and *velocity* fields to derive and visualize features in the spatial domain.

### 2.1 Isosurface-based Techniques

Prior analysis and visualizations of the Earth’s mantle convection data indicate scientists study the relationship of multiple attributes (temperature anomaly, density anomaly) using adjacent views for each attribute. We consider two strategies to produce a single view using bivariate data. The first approach we consider is isosurfaces with local coloring (Section 2.1.1). The second approach we consider is feature level-sets (Section 2.1.2). Although feature level-sets can be used to study multivariate data ( $n > 2$ ), we limit our analysis to bivariate data.

#### 2.1.1 Isosurfaces with Local Coloring

To visualize bivariate data using isosurfaces with local coloring, we use the first attribute to extract the surface geometry and the second attribute to locally color the surface geometry. Isosurfaces with local coloring provide insight into the feature structure defined by a single value (isovalue) of the first attribute as well as information pertaining to the variation of the second attribute on the feature surface via colormapping. We use this approach to visualize various combinations of attributes such as temperature anomaly, density anomaly, velocity magnitude and the derived finite-time Lyapunov exponent (FTLE).

---

\*e-mail: ssane@sci.utah.edu

†e-mail: tushar.athawale@gmail.com

‡e-mail: crj@sci.utah.edu

#### 2.1.2 Feature Level-Sets

Feature level-sets are the generalization of isosurfaces to multivariate data [5]. To extract feature level-sets from multivariate data in the spatial domain, a *trait*, analogous to an isovalue, is specified. The trait is defined in attribute space and can be of any dimension and structure (points, lines, intervals). For a given trait, a distance field is derived (based on a Euclidean distance metric) and mapped into the spatial domain. Level-sets of the derived distance field are called feature level-sets, and the “zero” level-set corresponds to the feature in the spatial domain that matches the trait exactly. We use bivariate data consisting of temperature anomaly and density anomaly, or temperature anomaly and velocity magnitude, to derive feature level-set distance fields.

**Discernable Feature Level-Sets** Although feature level-sets provide us with the capability to study multivariate data, there are certain limitations in regard to discernibility. A lack of discernability results in the inability to distinguish between points in the domain with equal distance to the trait in the final level-set rendering, i.e., there is a lack of insight regarding the contribution of each attribute to the distance value. We present a straightforward solution for bivariate data in this context. To improve discernibility, we compute an additional field, the *discernibility* field, that stores the difference of the normalized values of each attribute. Thus, the resulting field values are between  $[-1, 1]$ , with a value of zero indicating an equal contribution from both attributes for a given distance. Whereas, positive or negative values indicate a greater contribution from one of the attribute. Similar to using isosurfaces with local coloring, we use the feature level-set distance field as input for level-set extraction and encode the discernibility field using color on the feature surface.

### 2.2 Flow Visualization Techniques

To study flow patterns in the Earth’s mantle convection data, we employ two flow visualization techniques. First, we consider filtering integral curves (streamlines, pathlines) using various features associated with each integral curve. Second, we derive the finite-time Lyapunov exponent to approximate the stretching rates of particles and thus provide insight regarding mixing in the domain [4].

#### 2.2.1 Attributed-Filtered Integral Curves

We visualize integral curves computed using the entire time-varying vector field of the data set, as well as single time slices. In both cases, we encode an attribute or time along the trajectory using color.

**Streamlines** We compute streamlines using a single time slice of the data set. For each streamline, we accumulate information along the trajectory, such as curve distance, change in depth, temperature anomaly, and density anomaly. We place 100,000 random seed points and compute streamlines by performing 500 particle advection steps. Finally, we filter streamlines based on various criteria in order to minimize clutter and occlusion, while highlighting regions of interest in the domain.

**Pathlines** We compute pathlines using every cycle of the time-varying vector field data. Similar to above, for 100,000 randomly seeded particles, we integrate pathlines and accumulate information along the trajectory. As a final step, we filter pathlines based on attributes to isolate various flow patterns while reducing clutter and occlusion. We provide a visualization of pathlines in the supplementary material.

### 2.2.2 Finite-Time Lyapunov Exponent

The finite-time Lyapunov exponent is a scalar value that estimates the rate of stretching in the proximity of a particle over a fixed time interval. We visualize the FTLE scalar field using the technique described in Section 2.1.1.

### 2.3 Topological Data Analysis

Topological data analysis has proved effective in understanding complex simulations. Erlebacher et al. [3] characterized the Earth's mantle convection simulations with critical points as topology descriptors. The high complexity of simulations can result in a large number of critical points, therefore, rendering less effectiveness in extracting interesting patterns from data. We apply the idea of topology simplification [2] to critical points to gain insight into the prominent features of the dataset and study the evolution of those features. Topological simplification helps us reduce the number of critical points and analyze critical points that denote prominent/significant features of a scalar field. For our results presented in the supplementary material, we computed critical points of the temperature anomaly field and performed topology simplification using the topology toolkit (TTK) [12].

## 3 RESULTS

We discuss our results in the context of the tasks specified for the SciVis Contest. To visualize the correlations between variables and the flow patterns in the domain we employ analysis techniques that can be applied to multivariate/bivariate data. In Fig. 1, we visualize the correlation between the variables of temperature anomaly and spin transition-induced density anomaly as well as temperature anomaly and the derived FTLE (20 Myr integration time). In Fig. 1 (a), a scatterplot shows the relation between all three considered attributes. Negative spin transition-induced density anomalies are known to enhance mixing in the lower regions of the mantle and consequently enhance the vigor of rising plumes. These regions are observed in Fig. 1 (b) which shows the isosurface near the core mantle boundary. Additionally, visualizing the temperature anomaly isosurface colored by the density anomaly reveals the change of density anomaly along the rising plume structure.

Isosurfaces with local coloring also enable the visualization of stagnated or diverted cold slabs and hot plumes in Fig. 2 and Fig. 3, respectively. By encoding velocity magnitude using color, we are able to identify stagnated material at the depths of 660km and 1600km as white slab-like surfaces. For example, Fig. 2 (e) shows a cold slab that is horizontally extended at 1600km. By considering the behavior over 100 Myr, we are able to visualize the formation of cold slabs stagnating at mid-mantle depths as well as an avalanche. Fig. 3 uses a semi-opaque sphere at 1600km depth as reference to locate the stagnant hot plume (annotated in Fig. 3 (a)). In the animation provided in the supplementary material, the formation of superplumes is visualized as several individual plumes merge to produce large mantle upwellings.

As a second approach to address the challenge of study the correlations between variable and flow patterns, we visualized feature level-sets. Fig. 4 shows the *trait* (analogous to an isovalue) along with three level-sets extracted from the trait-specific distance field. A zero level-set would extract a feature in the spatial domain that exactly matches the trait. Level-sets using small threshold values extract the points *close to the feature in attribute space*. The trait

for our feature level-set studies the correlation between the temperature anomaly and spin transition-induced density anomaly. Given points that are of equal distance value in the spatial domain cannot be distinguished from one another using simple feature level-sets, we explore the use of an additional field to improve discernability in Figure 5. The feature level-set extracted shows hot rising plume structures as well as the ridges that spread across the core mantle boundary and form an interconnect. By considering the feature level-set, the variation in the density anomaly is visible along the vertical structure of the plume, while the variation in temperature anomaly is visible laterally for these structures and along the ridges.

Fig. 6 visualizes the domain using a flow visualization technique augmented with isosurfaces. We visualize two sets of integral curves: (1) streamlines passing through high temperature anomaly regions and colored by the local spin transition-induced density anomaly (Accent colormap), and (2) streamlines passing through low temperature anomaly regions and colored by the local temperature anomaly (RdBl colormap). Additionally, we filter streamlines by length and change in depth, prioritizing longer curves with large change in depth. The nested temperature anomaly isosurface (RdBl colormap) shows light blue isosurfaces in the upper mantle as well as a cylindrical structure around descending cold material (top of the figure). These integral curves travel laterally before descending into the lower mantle. The feature level-set (Reds colormap) intersects with the streamlines depicting the plumes. Additionally, flat structures of the feature level-set are visible in the upper mantle above the plumes indicating regions of high temperature anomaly and negative density anomaly exist. Overall, this flow visualization reveals the interaction between various features derived from by multiple attributes (temperature anomaly, spin transition-induced density anomaly, velocity).

## REFERENCES

- [1] S. Chen, H. Zhang, D. A. Yuen, S. Zhang, J. Zhang, and Y. Shi. Volume rendering visualization of 3d spherical mantle convection with an unstructured mesh. *Visual Geosciences*, 13(1):97–104, 2008.
- [2] H. Edelsbrunner, D. Letscher, and A. J. Zomorodian. Topological persistence and simplification. *Discrete and Computational Geometry*, 28:511–533, 2002.
- [3] G. Erlebacher, D. A. Yuen, and F. Dubuffet. Case study: Visualization and analysis of high rayleigh number-3d convection in the earth's mantle. In *IEEE Visualization, 2002. VIS 2002.*, pp. 493–496. IEEE, 2002.
- [4] C. G. Farnetani and H. Samuel. Lagrangian structures and stirring in the earth's mantle. *Earth and Planetary Science Letters*, 206(3-4):335–348, 2003.
- [5] J. Jankowai and I. Hotz. Feature level-sets: Generalizing iso-surfaces to multi-variate data. *IEEE Transactions on Visualization and Computer Graphics*, 26(2):1308–1319, 2020. doi: 10.1109/TVCG.2018.2867488
- [6] K. E. Jordan, D. A. Yuen, D. M. Reuteler, S. Zhang, and R. Haines. Parallel interactive visualization of 3d mantle convection. *IEEE Computational Science and Engineering*, 3(4):29–37, 1996.
- [7] H. Obermaier, M. I. Billen, H. Hagen, M. Hering-Bertram, and B. Hamann. Visualizing strain anisotropy in mantle flow fields. In *Computer Graphics Forum*, vol. 30, pp. 2301–2313. Wiley Online Library, 2011.
- [8] S. Schröder, J. A. Peterson, H. Obermaier, L. H. Kellogg, K. I. Joy, and H. Hagen. Visualization of flow behavior in earth mantle convection. *IEEE transactions on visualization and computer graphics*, 18(12):2198–2207, 2012.
- [9] M. Shahnas, D. Yuen, and R. Pysklywec. Mid-mantle heterogeneities and iron spin transition in the lower mantle: Implications for mid-mantle slab stagnation. *Earth and Planetary Science Letters*, 458:293–304, 2017. doi: 10.1016/j.epsl.2016.10.052
- [10] M. H. Shahnas, W. R. Peltier, Z. Wu, and R. Wentzcovitch. The high-pressure electronic spin transition in iron: Potential impacts upon man-

- tle mixing. *Journal of Geophysical Research: Solid Earth*, 116(B8), 2011. doi: 10.1029/2010JB007965
- [11] M. H. Shahnas, R. N. Pysklywec, and D. A. Yuen. Spawning superplumes from the midmantle: The impact of spin transitions in the mantle. *Geochemistry, Geophysics, Geosystems*, 17(10):4051–4063, 2016. doi: 10.1002/2016GC006509
- [12] J. Tierny, G. Favelier, J. A. Levine, C. Gueunet, and M. Michaux. The topology toolkit. *IEEE Transactions on Visualization and Computer Graphics*, (1):832 – 842, Jan 2018.
- [13] M. Yoshida. Core-mantle boundary topography estimated from numerical simulations of instantaneous mantle flow. *Geochemistry, Geophysics, Geosystems*, 9(7), 2008.

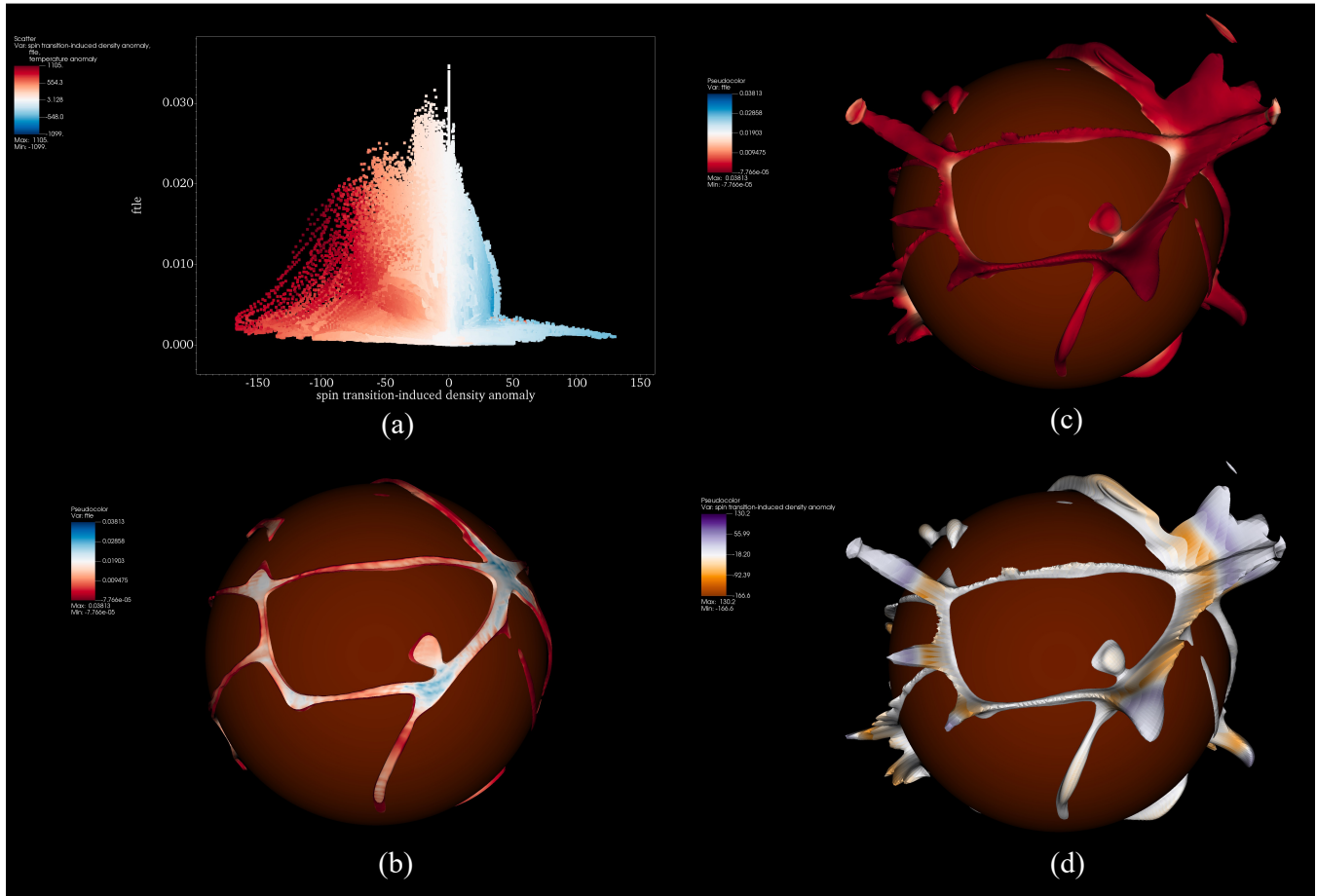


Figure 1: An example demonstrating isosurfaces with local coloring using the first time step of the Earth's mantle convection data set. We use three attributes: temperature anomaly, spin transition-induced density anomaly, and the finite-time Lyapunov exponent (FTLE). Figures (b), (c), and (d) use the same viewpoint. (a) Scatterplot of FTLE (y-axis) and spin transition-induced density anomaly (x-axis), with temperature anomaly encoded using color. The scatterplot shows higher FTLE values for negative spin transition-induced density anomaly and high temperature anomaly. (b) Isosurface of temperature anomaly at 300K using color to encode the local FTLE values on the surface. The integration time for the FTLE approximation is 20 Myr. We only compute the isosurface between the core mantle boundary and a depth of 2700km. This allows us to observe the approximation of fluid separation at the base of the plumes. (c) Similar to (b), with the isosurface computed between the core mantle boundary and a depth of 600km. With the plume structure now visible, FTLE values appear higher at the base of the plume. (d) Isosurface of temperature anomaly at 300K using color to encode the local spin transition-induced density anomaly values on the surface. The density anomaly varies greatly along vertical plume structure. Negative density anomalies play a role in mixing and accelerating rising material from the core mantle boundary.



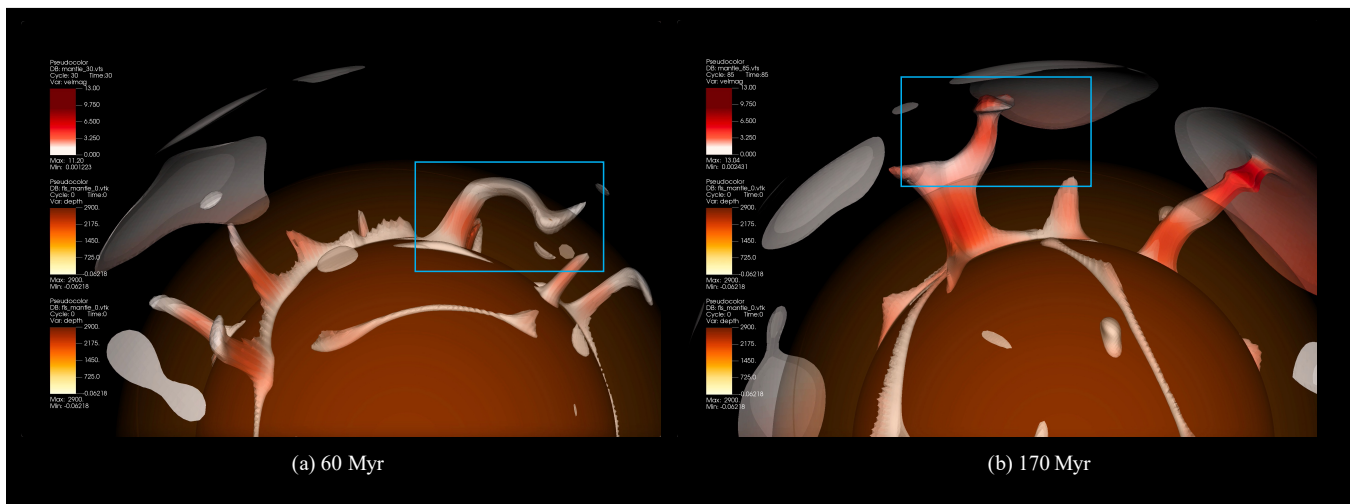


Figure 3: Visualization of stagnant or diverted hot plumes at two time steps. We visualize three nested semi-opaque isosurfaces of temperature anomaly (300K, 400K, 500K). The isosurfaces are locally colored by velocity magnitude. Very low velocity magnitude values result in white isosurfaces and indicate hot stagnant or diverted material, whereas orange/red isosurfaces indicate hot rising material. In addition to the opaque sphere at the core mantle boundary depth, we visualize a semi-opaque sphere to show 1600km depth. (a) At 60 Myr, we visualize stagnant/diverted hot plume material at 1600km. (b) At 170 Myr, we visualize hot material rising to upper mantle depths. An animation of the entire time series shows the formation of several plumes and is provided as supplementary material.

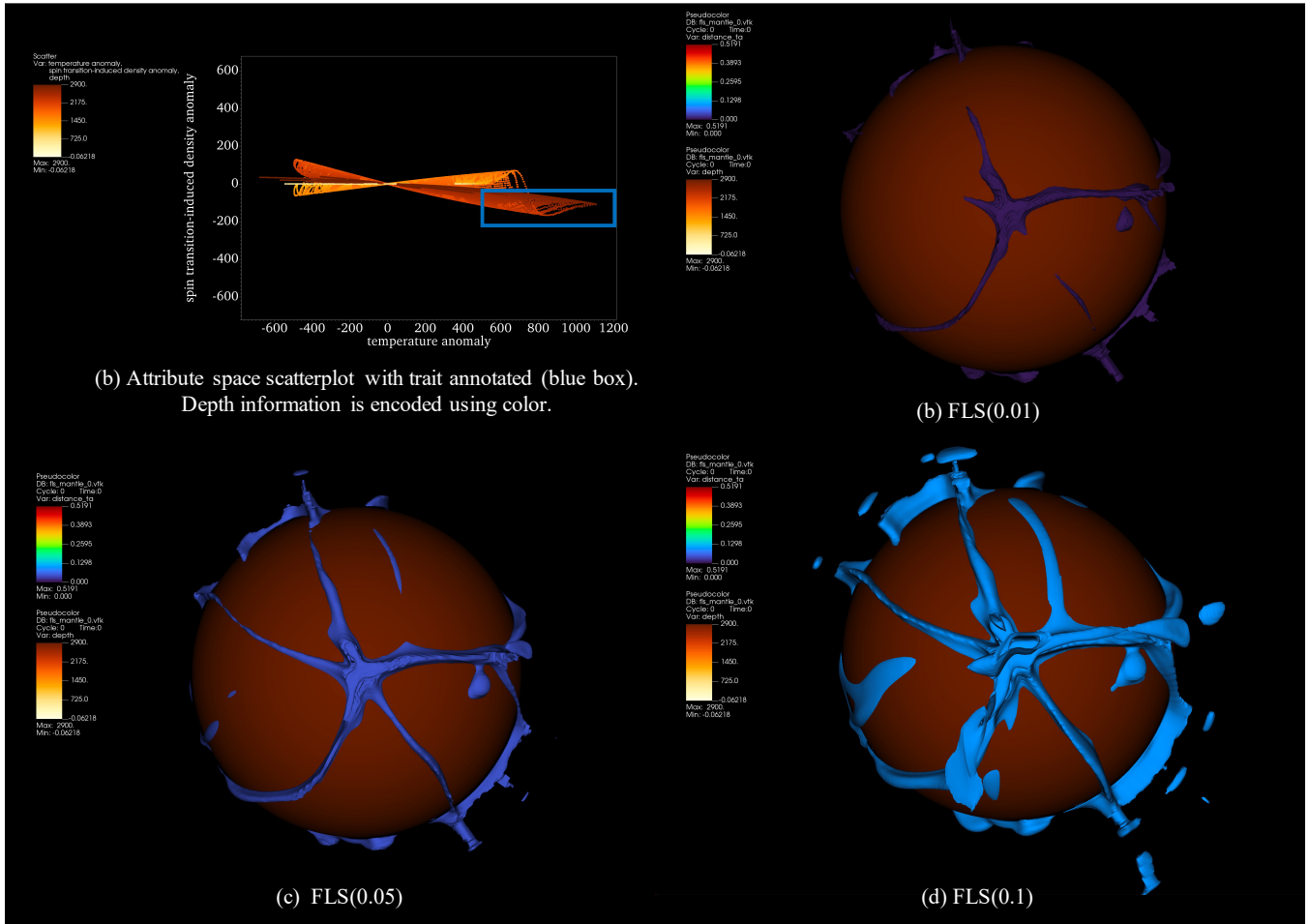


Figure 4: Visualization of hot ridge structures near the core mantle boundary using feature level-sets. We use the attributes of spin transition-induced density anomaly and temperature anomaly to define the trait. The attribute space scatterplot in (a) shows the trait definition. We select our feature in attribute space as a region with high temperature anomaly and negative spin transition-induced density anomaly. A distance field (Euclidean distance metric) is computed in attribute space using normalized field values before pulling back the distance field to the spatial domain. We extract three feature level-sets from the distance field. Specifically, we visualize levels 0.01, 0.05, and 0.1. We select values closer to zero in order to extract features that closely match our trait definition. We denote each level-set as  $\text{FLS}(X)$  where  $X$  is the level.  $\text{FLS}(0.01)$  in (b) visualizes disconnected bases of transient plumes.  $\text{FLS}(0.05)$  visualizes a network of ridge structures with plume formations at intersections. In  $\text{FLS}(0.1)$ , as we move further away from the exact definition of the trait, we see disjoint features above the ridges. This reflects the change in density anomaly in plumes rising from the core mantle boundary.

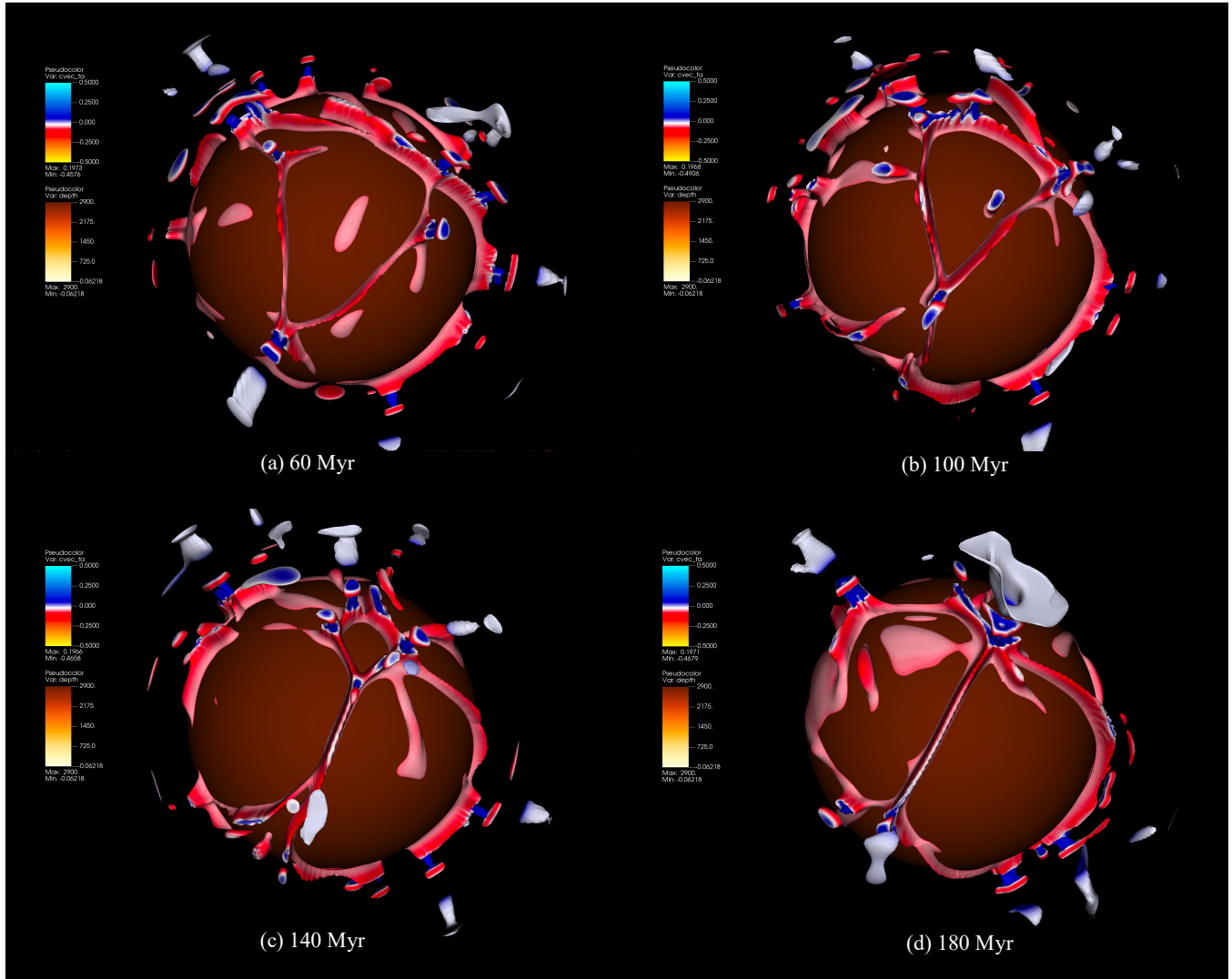


Figure 5: Visualization of discernable feature level-sets showing regions of high temperature anomaly and negative spin transition-induced density anomaly. For non-zero level-sets, there is a lack of discernability regarding the composition of the equal distance points in the domain. To address this, we derive an additional field that encodes the difference of absolute normalized values of two attributes to locally color the surface. In the visualization above, white regions of the isosurface indicate an equal contribution from both attributes to the distance. For the level-set selected above, red regions (negative values) of the isosurface indicate the temperature anomaly contributes to the distance values, whereas blue regions (positive values) indicate the density anomaly contributes to the Euclidean distance from the trait. Across time steps ridge structures constantly evolve and release hot plumes that undergo significant changes in density anomaly. An animation of the discernable feature level-sets across all 500 Myr is provided in the supplementary material.

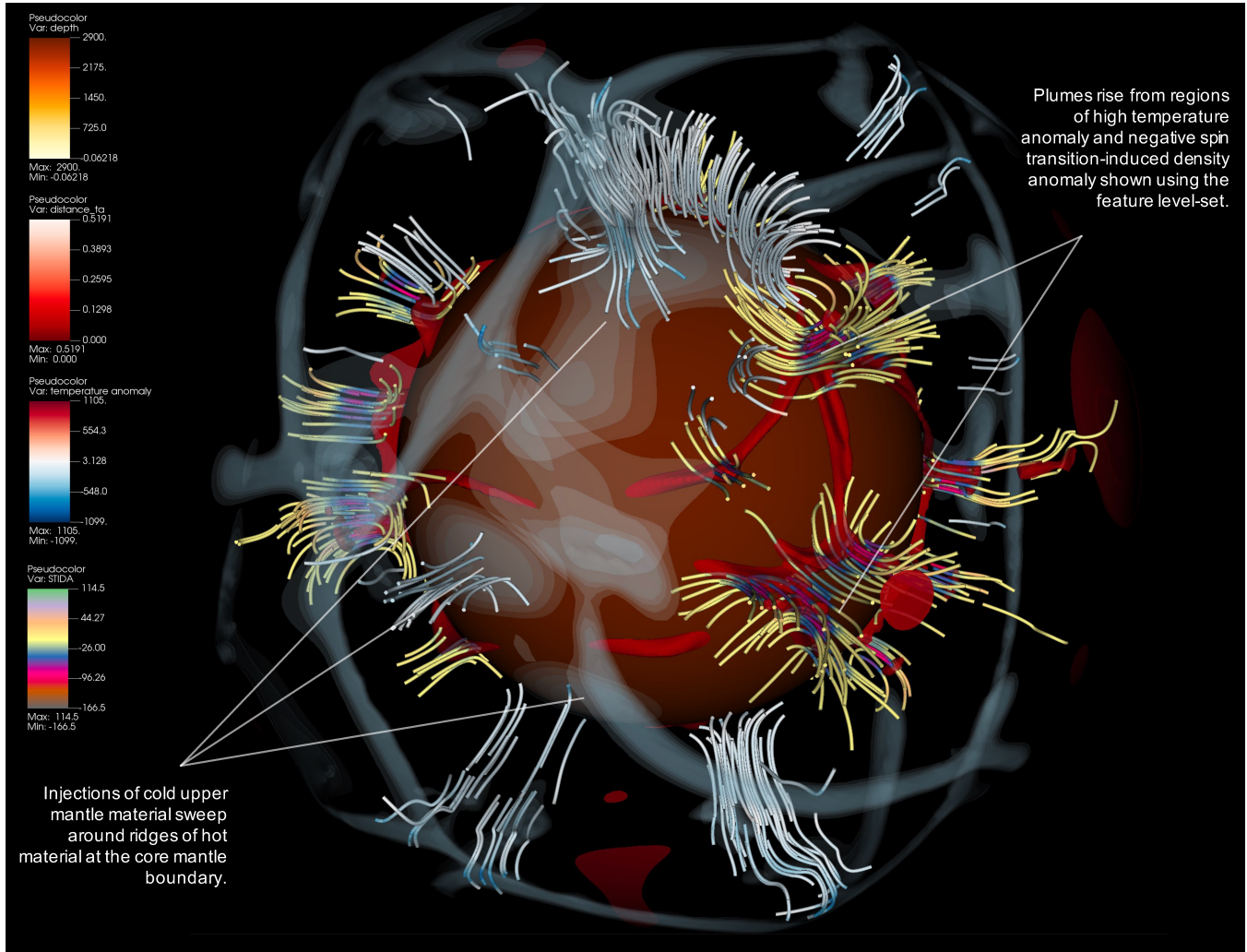


Figure 6: Flow visualization using attribute-filtered integral curves augmented by semi-opaque nested isosurfaces and a feature level-set. We compute integral curves (streamlines) and accumulate feature information, such as change in depth, curve length, maximum and minimum temperature anomaly, as well as temperature and density anomaly at each sample point along the curve, at the time of integration. Next, we filter integral curves to highlight regions of interest - integral curves that experience extremes of temperature anomaly and satisfy a change in depth criteria. Integral curves visualizing sinking material are colored by temperature anomaly and integral curves visualizing hot rising plumes are colored by spin transition-induced density anomaly. The significant changes in density anomaly are visible along the curves. Additionally, we visualize nested isosurfaces of negative temperature anomaly and a feature level-set as described in Figure 4. Plume structures are visible at the intersections of the ridges seen via the feature level-set. Isosurfaces of temperature anomaly (-200K to -400K) show cold material on the core mantle boundary where sinking integral curves descend.